Emotion Feature Analysis and Recognition Based on Reconstructed EEG Sources

GUIJUN CHEN[ID], XUEYING ZHANG[ID], (Member, IEEE), YING SUN[ID], AND JING ZHANG

College of Information and Computer, Taiyuan University of Technology, Taiyuan 030024, China

Corresponding authors: Guijun Chen (chenguijun@tyut.edu.cn) and Xueying Zhang (tyzhangxy@163.com)

ABSTRACT Emotion plays a significant role in perceiving external events or situations in daily life. Due to ease of use and relative accuracy, Electroencephalography (EEG)-based emotion recognition has become a hot topic in the affective computing field. However, scalp EEG is a mixed-signal and cannot directly indicate the exact information about active cortex sources of different emotions. In this paper, we analyze the significant differences of active source regions and frequency bands for pairs of emotions-based reconstructed EEG sources using sLORETA, and 26 Brodmann areas are selected as the regions of interest (ROI). And then, six kinds of time- and frequency-domain features from significant active regions and frequency bands are extracted to classify different emotions using support vector machines. Furthermore, we compare the classification performances of emotion features extracted from active source regions and EEG sensors. We have demonstrated that the features from selected source regions can improve the classification accuracy by extensive experiments on the DEAP and TYUT 2.0 EEG-based datasets.

INDEX TERMS Emotion recognition, EEG source reconstruction, inverse solution, difference analysis of active source, time- and frequency-domain features.

I. INTRODUCTION

Emotion is the human affective response to the external event or specific situation, which plays a significant role in daily life. If a person can't correctly perceive and regulate emotions, it will become very terrible. For example, as a mood disorder, depression usually causes severe symptoms that affect one's feeling, sleeping and even thinking. Besides, if we can endow a machine with emotion, it will significantly improve the efficiency of the human-machine interaction. Therefore, analyzing the emotion mechanism and automatic recognition of emotion state has become a hot topic in psychology, medicine and computer science in recent years [1], [2].

In General, it is believed that people have six basic emotions [3], including anger, disgust, fear, happiness, sadness, and surprise. Besides this discrete emotion, there is a continuous model [4], which can be described in a 2-dimensional

The associate editor coordinating the review of this manuscript and approving it for publication was Jihad Aljaam[ID].

space with dimensions valence and arousal (see Fig. 1) or even with third dimension dominance. Early studies about human emotion mainly focused on facial expressions, speech and gestures, which are the external signs of emotion. That is, we can often perceive a person's happy or sad emotion from facial expression and speech. But these feelings can be controlled by people, and their real emotions will be masked. Thus, the current researches about emotion mainly focus on physiological signals [5], [6], e.g. galvanic skin response (GSR), heart rate (HR), electroencephalography (EEG), magnetoencephalography (MEG) and functional magnetic resonance imaging (fMRI) and so on. These can give some objective indicators of emotion. The GSR and HR mostly reveal the arousal information, while EEG, MEG and fMRI have to do with the neurocognitive process of the brain. Especially, EEG is of increasing interest, because of its non-invasiveness and the relative ease of use. Another critical advantage of EEG is its high temporal resolutions, which can characterize the dynamic response of different emotions in the millisecond level.
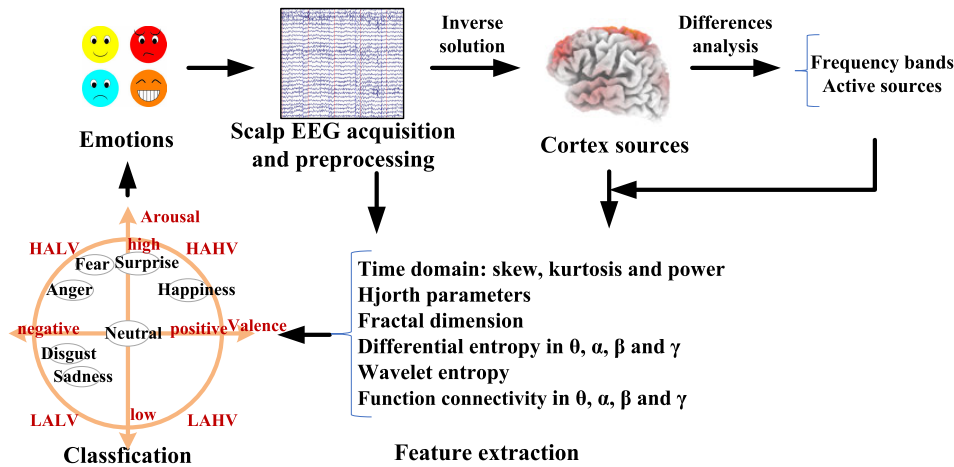
FIGURE 1. Schematic diagram of our framework.

Currently, researches on EEG emotion recognition focus on selecting the optimal channels or features from raw EEG, which can notably improve the emotion recognition accuracy [7], [8]. However, scalp EEG is a mixed-signal from multiple cortex sources through some tissues. It cannot directly indicate the exact information about active sources of different emotions in the brain. Many various sources may generate the same distribution on the scalp because of the volume conductor and field spread effects [9].

To localize the active sources, we commonly employ the method to compute the inverse solution, which is the estimation of an equivalent dipole or current density on predefined surfaces or a three-dimensional volume with a priori assumption [10]. Initially, EEG source reconstruction was used as a useful technique to localize the epileptic focus non-invasively [11]. Due to non-uniqueness of the inverse solutions, the head model-based forward and inverse problems were studied. Some source estimation algorithms have been proved to be reliable, including least square fit, multiple signal classification, minimum norm, local autoregressive average, Bayesian approaches and low-resolution brain electromagnetic tomography (LORETA) [12]. Keil *et al.* [13] investigated the time course and source distribution of emotional picture processing using minimum norm method. They localized the sources of slow-wave modulation in occipital and posterior parietal cortex with a right-hemispheric dominance. Keuper *et al.* [14] reconstruct the current-density sources for two early time intervals P1 and early posterior negativity (EPN) to understand the spatiotemporal brain dynamics underlying emotional-word processing by using L2-minimum norm estimate and realistic head models.

Further, Kashyap *et al.* [15] performed the source location of EEG and functional connectivity for the DEAP emotional dataset by using standard LORETA (sLORETA) tool. The results showed that there were different active regions with different current densities for different emotional states. Becker *et al.* [16] presented a new 257-channel

EEG emotion database and reconstructed the cortical activity by applying the regularized least-squares WMNE algorithm. And the features were extracted from source regions and EEG channels. The results showed that the source reconstruction improved the valence classification performance. Padilla-Buritica *et al.* [17] proposed a method for emotion classification that relied on features extracted from the active brain areas, including power spectral density, Wavelet, and Hjorth parameters. Obtained results on the DEAP database showed that source estimation by employing the multiple sparse priors (MSP) can improve the accuracy of discrimination. In [18], sLORETA was used to localize regions involved in different emotions of DEAP dataset. Seven frequency bands were computed to evaluate gender differences for emotional responses.

In summary, EEG source localization procedure can exploit the available spatiotemporal information for emotion recognition. However, the problem of field spread is never wholly abolished in source space with inverse solution currently. A better strategy could be to analyze the active changes for different emotions, rather than the active strength [19]. Most of the works did not focus on the significant differences of active sources between pairs of emotions. No study has yet been conducted to systematically explore the cortex regions of interest (ROI) mapping from EEG for different emotions. Therefore, the principal goals of this study are to analyze the differences of cortical ROI among emotion tasks and extract the emotion-based recognizable features from the active sources. As shown in Fig. 1, our work is made up of three parts as follows. For the preprocessed emotion-based EEG data, first, the sLORETA tool is applied to obtain the inverse solutions of EEG sources and analyze the significant differences of active source regions and frequency bands between pairs of emotions. The source regions and frequency bands of interest are determined. Second, six kinds of features from both significant active source space and sensor space are extracted to classify different emotions. Finally, the

classification performances of emotion features extracted from active source regions are compared with the ones from EEG sensors.

This paper is organized as follows: In Section II, we describe the emotion datasets and the source localization steps, the types of features, and the classification approach that we consider in this paper. Section III presents and discusses the classification results that we have obtained on two datasets. These results are summarized, and conclusions are drawn in Section IV.

II. MATERIALS AND METHODS

A. EEG-BASED EMOTION DATASETS

In this work, the emotion EEG signals from DEAP [20] and TYUT 2.0 [21] datasets were used to evaluate the performance of source localization and emotion recognition. The DEAP dataset includes 32-channel EEG signals of 32 subjects for 40 trials. During each trial, the subject was required to watch a one-minute excerpt of music videos and rate it in terms of valence, arousal, dominance, liking with the distributed scores from 1 to 9. Herein, the emotion states are categorized into four classes including HALV, HAHV, LALV and LAHV according to valence-arousal scores, where the score greater than five labels high (H) and the score less than five labels low (L). The EEG signals were downsampled to 128 Hz and the EOG artifacts were removed with a blind source separation technique. A 4.0-45 Hz band-pass filter, common average reference and 3s baseline correction were applied to data preprocessing. And then, a 5 s hamming window with non-overlap was used to divide each signal into 12 data segments.

The TYUT 2.0 dataset from our laboratory was recorded with 1000 Hz sampling rate by using the 64-channel Neuroscan system. We selected the EEG data from 16 subjects for 250 trials with five classes of emotions, including sadness, anger, happiness, surprise and neutral. Each emotion had 50 trials, and each speech clip was only presented once at each trail. The EOG artifacts were removed by using independent component analysis. The 0.5-45 Hz band-pass filter and bilateral mastoid reference were applied to data preprocessing. A 1s hamming window was used to extract an event-related data frames from -0.2s to 0.8s, and 0.2s baseline correction was applied. The detailed information about these two publicly available datasets is shown in Table1. The placement of the electrodes is depicted in Fig. 2, and the considered electrodes in DEAP dataset are marked in black.

B. RECONSTRUCTED EEG SOURCES OF EMOTIONS

As a mixture signal, the scalp EEG of emotional response cannot be interpreted straightforward. To assess the active brain regions, we should project the EEG data on the source space, which can be modelled by a high number of current dipoles with fixed locations and orientations as follows,

$$X = KS + \varepsilon \qquad (1)$$

TABLE 1. Description of EEG-based emotion datasets.

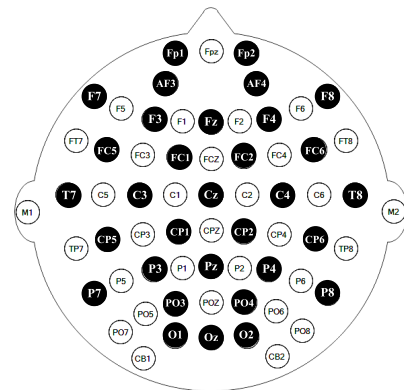| Dataset	Emotions	Stimulus (duration)	#Subjects(F/M)	EEG signal
DEAP	HALV, HAHV, LALV, LAHV	music video (60 sec)	32(16/16)	32-channel 128 Hz
TYUT 2.0 Emotion EEG	sadness, anger, happiness, surprise and neutral	speech (0.5-3 sec)	16(8/8)	64-channel 1000 Hz

FIGURE 2. 10/20 Electrode Positions.

where $X \in R^{C \times T}$ is EEG signal with C channels and T time samples, $S \in R^{N \times T}$ is the N distributed current dipoles perpendicular to the cortical surface, ε is the noise from measurement system and background activity of the brain. In this case, $K \in R^{C \times N}$ is defined as the lead-field matrix from sensor space to source space, which can be computed for a given head model and is thus known. However, the number of scalp sensors is usually much less than the number of current dipoles, i.e. $C \ll N$, the lead field matrix is severely underdetermined. So it is necessary to make some additional constraint assumptions for the source current dipoles to solve this ill-posed inverse problem. The commonly employed assumption is that the spatial distribution energy of source is limited, and then the solution of the inverse problem can be transformed into the following optimization problem,

$$\min_{K, \varepsilon} \|X - KS - \varepsilon\|^2 + \lambda \|S\|^2 \qquad (2)$$

where $\lambda \geq 0$ is a regularization parameter. This optimization problem is similar to the regularized least-squares function, which can be solved by sLORETA method with little running time and zero location error [22]–[24]. The specific solution to this optimization problem is as follows.

$$\hat{S} = TX \qquad (3)$$

where $T = K^T H \left[HKK^T H + \lambda H \right]^+$, $H = I - 11^T /1^T 1 \in R^{C \times C}$ is the centering matrix, $I \in R^{C \times C}$ is the identity matrix, $1 \in R^{C \times 1}$ is a vector of ones; and $[]^+$ denotes the pseudoinverse.
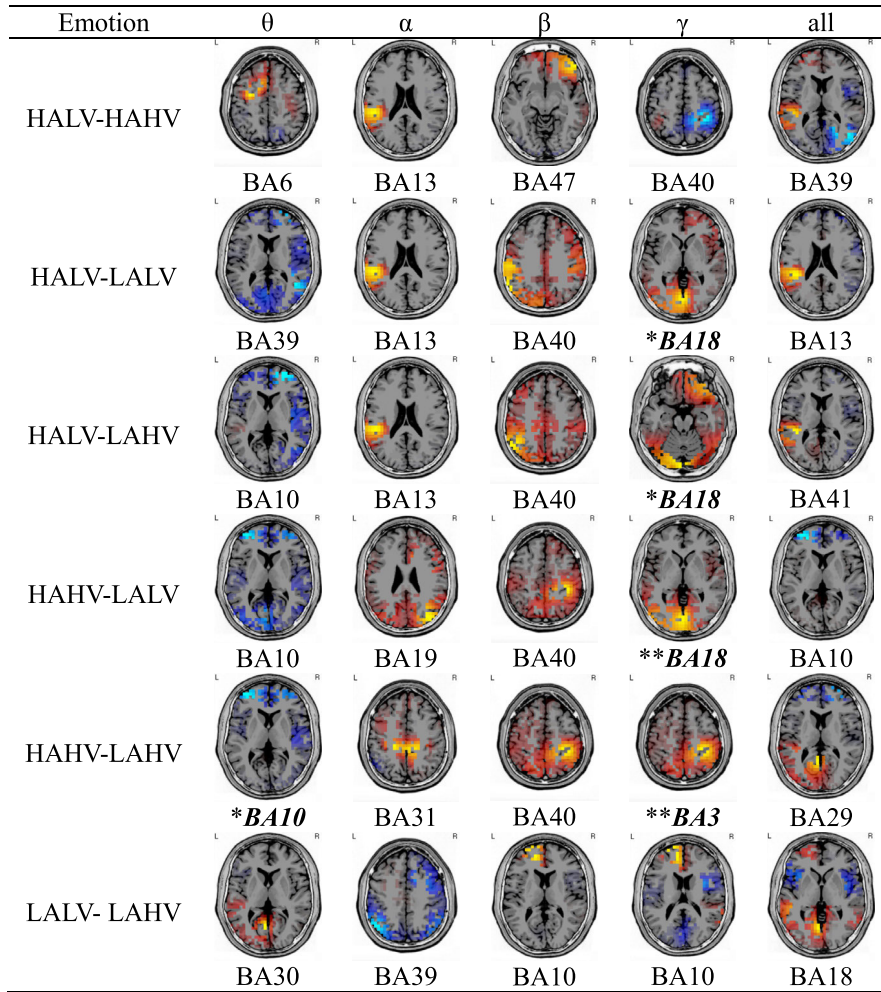
Emotion	θ	α	β	γ	all
HALV-HAHV	BA6	BA13	BA47	BA40	BA39
HALV-LALV	BA39	BA13	BA40	*BA18	BA13
HALV-LAHV	BA10	BA13	BA40	*BA18	BA41
HAHV-LALV	BA10	BA19	BA40	**BA18	BA10
HAHV-LAHV	*BA10	BA31	BA40	**BA3	BA29
LALV- LAHV	BA30	BA39	BA10	BA10	BA18

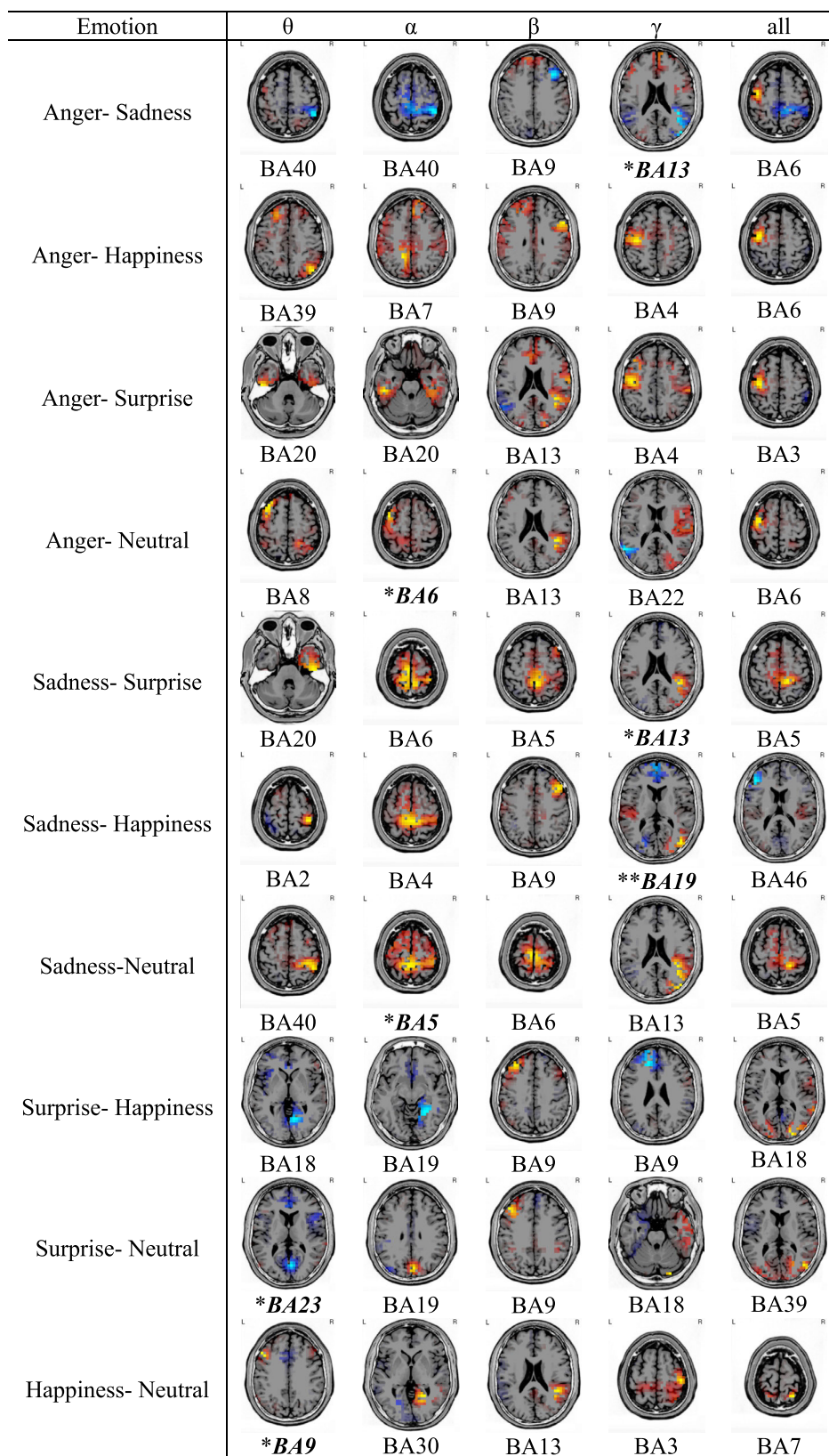**FIGURE 3.** Differences of active brain sources for DEAP emotion dataset (∗ p<0.05, ∗∗ p<0.01).

In this study, we investigated the significant differences of active brain sources for four EEG frequency bands by different kinds of emotion's stimulus. The EEG frequency bands, including θ (4-8 Hz), α (8-13 Hz), β (13-30 Hz), and γ (30-45 Hz) were computed using the least-squares FIR bandpass filter. The sLORETA was used to obtain the cortical distribution of current density for the emotion EEG and to compare the difference among emotion responses using paired samples t-test. We used a three-shell spherical head model with the Colin27 brain atlas template from Montreal Neurological Institute (MNI) and produced 6239 cortical grey matter voxels at 5mm resolution in MNI coordinates. Neither data normalization nor the baseline correction was performed. The t-test was carried out for a log of the ratio of averages (log of F-ratio), and the randomization statistical nonparametric mapping (SnPM) was performed to compute critical thresholds and p values. The number of randomizations was set to 5000.

Fig. 3 and Fig. 4 summarize the differences of active brain sources for above mentioned two EEG emotion datasets with four frequency bands respectively. The source location difference between any pair of emotions can be observed in cortical level and Brodmann areas (BA). For the DEAP dataset, the results show significant differences between pairs of emotions in BA3, 18 and 10 for γ and θ frequency bands with p<0.05. These areas mainly involve the postcentral gyrus, anterior prefrontal cortex and occipital visual cortex, which are related to emotional perception and processing. This viewpoint is consistent with the results in [25], [26]. For example, BA3 has been implicated in the perception of emotions based on vocal prosody, BA10 is related to dealing with emotional stimuli, and BA18 responses to emotion in visual processing. Other active regions of emotion mainly include BA6, 13, 19, 29, 30, 31 39, 40, 41 and 47. In addition, the significant differences might be determined by arousal, i.e. response to different emotions are affected by high arousal (HA) and low arousal (LA), and the effect of valence is smaller compared with arousal. This result is consistent with [27].

Therefore, extracting valence-related features is essential to distinguish different emotions.

For the TYUT 2.0 Emotion dataset, the results show significant differences between pairs of emotions in BA5, 6, 9, 13, 19 and 23 from θ, α and γ frequency bands with

Emotion	θ	α	β	γ	all
Anger- Sadness	BA40	BA40	BA9	*BA13*	BA6
Anger- Happiness	BA39	BA7	BA9	BA4	BA6
Anger- Surprise	BA20	BA20	BA13	BA4	BA3
Anger- Neutral	BA8	*BA6*	BA13	BA22	BA6
Sadness- Surprise	BA20	BA6	BA5	*BA13*	BA5
Sadness- Happiness	BA2	BA4	BA9	**BA19**	BA46
Sadness-Neutral	BA40	*BA5*	BA6	BA13	BA5
Surprise- Happiness	BA18	BA19	BA9	BA9	BA18
Surprise- Neutral	*BA23*	BA19	BA9	BA18	BA39
Happiness- Neutral	*BA9*	BA30	BA13	BA3	BA7

FIGURE 4. Differences of active brain sources for TYUT 2.0 emotion dataset (∗ $p<0.05$, ∗∗ $p<0.01$).

TABLE 2. Features applied in this paper.

Features	number
Time domain (TD): skew, kurtosis and power	$3N$
Hjorth parameters (HP)	$2N$
Fractal dimension (FD)	N
Differential entropy (DE) in θ, α, β and γ	$4N$
Wavelet entropy (WE)	N
Function connectivity (FC) features in θ, α, β and γ	16

p<0.05. Other active regions of emotion mainly include BA3, 7, 8, 18, 20, 29, 30, 39 and 40. Similar to DEAP dataset, significant differences mainly occur between high arousal and low arousal emotions, such as anger- sadness, sadness-happiness and sadness-surprise.

Above all, though all BA regions contribute to the measured EEG signals, only part of them will be involved in processing emotions. For further analysis and feature extraction, we consider 26 Brodmann areas as the region of interest (ROI) which have been observed from the above results. The selected ROI sets include BA3, 5, 6, 9, 10, 13, 18, 19, 23, 29, 30, 39 and 40 with bilateral hemispheres. And then, the volume current density of the active source is assigned to each ROI based on the nearest neighbor principle, and the current density of each ROI is obtained, from which the features were to be extracted.

C. FEATURE EXTRACTION

In this paper, we consider six kinds of features extracted from time, frequency and time-frequency domains that have been widely used to emotion recognition [28]. All features are computed in both the sensor space and source space, where corresponding signal series in the following equations are all called $x(t)$. The features applied in this paper are listed in Table 2 and are described as follows, where N is the number of sensors or source ROI regions.

1) TIME DOMAIN FEATURES

To measure the variability of signal amplitude in the time domain, we consider a set of classical statistical quantities as features, comprising skewness, kurtosis and total power of the signals. These quantities are defined below:

$$
\text{skewness} = \frac{\frac{1}{T}\sum_{t=1}^{T}(x(t)-\overline{x})^3}{\sigma^3} \tag{4}
$$

$$
\text{kurtosis} = \frac{\frac{1}{T}\sum_{t=1}^{T}(x(t)-\overline{x})^4}{\sigma^4} \tag{5}
$$

$$
\text{power} = \frac{1}{T}\sum_{t=1}^{T}x^2(t) \tag{6}
$$

where T is the length, $\overline{x}$ is the mean value and σ is the standard deviation of signal $x(t)$ respectively.

2) HJORTH PARAMETERS

Hjorth parameters can describe the statistical characteristics of signals in the time- or frequency-domains. They consist of Activity, Mobility, and Complexity descriptors [8], which are computed as:

$$
Activity = \sigma^2 = \frac{1}{T-1}\sum_{t=1}^{T}(x(t)-\overline{x})^2 \tag{7}
$$

$$
Mobility = \sigma_d/\sigma \tag{8}
$$

$$
Complexity = \frac{\sigma_{dd}/\sigma_d}{\sigma_d/\sigma} \tag{9}
$$

where σ_d represents the standard deviation of the first derivative of $x(t)$ and σ_{dd} represents the standard deviation of the second derivative of $x(t)$.

The Mobility parameter is proportional to a standard deviation of the power spectrum. It is an estimate of the mean frequency. The Complexity gives an estimate of the bandwidth of the signal, which indicates the similarity of the shape of the signal to a pure sine wave.

3) FRACTAL DIMENSION

Fractal dimension (FD) is a measure of signal complexity and irregularity. The value of FD is invariant, even under different initial conditions and amplitudes. The larger the value of FD, the more complicated the signal is. Therefore, the emotion evoked signal is typically characterized by a dynamic and non-stationary spectrum which accounts for higher FD. Due to much higher accuracy than other methods, Higuchi's algorithm is used to estimate the FD herein [29]. Consider the signal $x(t)$ with length T to be analyzed, construct a new time series.

$$
x_k^m = x\left(m+\left\lfloor\frac{N-m}{k}\right\rfloor k\right), \quad m = 1, 2\cdots k \tag{10}
$$

where m indicates the initial value, k is the time interval between points, and $\lfloor\cdot\rfloor$ means integer part. For each of the time series x_k^m, the average length is computed as

$$
\begin{aligned}
&L_m(k) \\
&= \left\{\left(\sum_{i=1}^{\lfloor(T-m)/k\rfloor}|x(m+ik)-x(m+(i1)k)|\right)\frac{T-1}{\lfloor(T-m)/k\rfloor k}\right\}/k
\end{aligned} \tag{11}
$$

If the average value over k sets of $L_m(k)$ is defined as $\langle L(k)\rangle \propto k^{-D}$, then the curve of $\ln(\langle L(k)\rangle)/\ln(1/k)$ is fractal with the dimension D, i.e. the slope of the least squares linear fit is the estimate of the fractal dimension D.

4) DIFFERENTIAL ENTROPY

Differential entropy (DE) can be used to measure the complexity of signal, which can be expressed as follows,

$$
\begin{aligned}
h(x) &= -\int_{-\infty}^{\infty}\frac{1}{\sqrt{2\pi\sigma^2}}e^{-\frac{(x-\mu^2)}{2\sigma^2}}\log\left(\frac{1}{\sqrt{2\pi\sigma^2}}e^{-\frac{(x-\mu^2)}{2\sigma^2}}\right)dx \\
&= \frac{1}{2}\log\left(2\pi e\sigma^2\right)
\end{aligned} \tag{12}
$$

where the signal series x should satisfy the Gaussian distribution with $N\left(\mu, \sigma^2\right)$. It has been proved that the sub-band signals can meet Gaussian distribution hypothesis [30], so the DE features were computed in 4 frequency bands mentioned above.

5) WAVELET ENTROPY

The wavelet analysis is an excellent way to describe the multi-scale and time-frequency local property with an optimal time-frequency resolution. Wavelet entropy can reflect the degree of signal variation, and it can provide useful information about the underlying dynamical process associated with the signal [31]. For the signal $x(t)$, if the wavelet decomposition is carried out at kth point with jth decomposition scale, the high-frequency coefficient $cD_j(k)$ and low-frequency coefficient $cA_j(k)$ can be obtained. And then the original signal $x(t)$ can be expressed as the sum of the reconstructed signal components $D_j(k)$ and $A_j(k)$ as follows [32]:

$$x(t) = D_1(t) + A_1(t) = D_1(t) + D_2(t) + A_2(t)$$
$$= \sum_{j=1}^{m} D_j(t) + A_m(t) \quad (13)$$

where the frequency band of $D_j(k)$ and $A_j(k)$ are $[2^{-j}f_s, 2^{-(j-1)}f_s]$ and $[0, 2^{-j}f_s]$ respectively, $j = 1, 2 \cdots, m$, f_s is the signal frequency.

Let's write $A_m(t)$ as $D_{m+1}(t)$,

$$x(t) = \sum_{j=1}^{m+1} D_j(t) \quad (14)$$

For the wavelet energy spectrum of $x(t)$,

$$E_j = \sum_{k} \left|D_j(k)\right|^2 \quad (15)$$

The total wavelet energy E is equal to the sum of the component energy spectrum E_j based on the characteristics of wavelet transform.

Let $p_j = E_j/E$, then the wavelet entropy is defined as

$$WE = -\sum_{j} p_j \log p_j \quad (16)$$

6) FUNCTION CONNECTIVITY FEATURES

Emotion responses in the brain depend on the coordination of multiple cerebral cortex regions. It is crucial that the brain is viewed as a complex network to obtain the functional connectivity characterizes between sensors or source regions. Conventional functional connectivity analyses exploit measurements from coherence, correlation, phase locking value (PLV) and phase lag index (PLI) [33], [34]. In this study, we used the PLI to describe the functional connectivity, which is more robust and can address the problem of volume conduction and active reference electrodes [35], [36]. The PLI is computed based on the instantaneous phases

$\phi_i(t)$ and $\phi_j(t)$ at brain regions i and j,

$$PLI(i, j) = \left| \frac{1}{T} \sum_{t=1}^{T} sign\left(\phi_i(t) - \phi_j(t)\right) \right| \quad (17)$$

where $sign()$ is the symbolic function, the range of PLI is between 0 and 1. To compute the instantaneous phases $\phi(t)$, the analytical signal $z(t)$ based on the Hilbert transform is used,

$$z(t) = x(t) + i\tilde{x}(t) = A(t) e^{i\phi(t)} \quad (18)$$

where $\tilde{x}(t)$ is the Hilbert transform of $x(t)$,

$$\tilde{x}(t) = \frac{1}{\pi} PV \int_{-x}^{\infty} \frac{x(\tau)}{t - \tau} d\tau \quad (19)$$

where PV refers to the Cauchy principal value. The instantaneous phase $\phi(t)$ can be computed by

$$\phi(t) = \arctan \frac{\tilde{x}(t)}{x(t)} \quad (20)$$

Once the PLI matrix between pairs of brain regions is obtained, the functional network with four frequency bands can be constructed with a collection of nodes (brain regions) and edges (PLI values). And then, the network properties, including characteristic path length L, clustering coefficient C, global efficiency E and local efficiency E_{loc}, are calculated as feature vectors to classify different emotions [37].

D. CLASSIFIER AND EVALUATION

To compare the performance of emotion recognition, we employed the support vector machines (SVM) classifier with Gaussian kernel, which can approximate most kernel functions if the kernel parameter was chosen appropriately [38]. The goal of SVM is to find a separating hyper-plane with maximum margins and classify the data accurately. There are two parameters, including penalty parameter and the kernel parameter, that need to be optimized to improve the classification accuracy [39]. The grid search method was utilized to tune the parameters, which were searched in the range from 2^{-8} to 2^8. The classification performance was assessed in terms of the average accuracy (AC) and standard deviation (SD) using 10-fold cross-validation.

III. EXPERIMENTS AND RESULTS ANALYSIS

In this section, we compare and analyze the classification performance for different features extracted from both sensors and source regions in two emotion datasets. The experiments were performed in a PC with the MATLAB R2014a development environment. The SVM classifier was based on LIBSVM 2.89 toolbox [40]. We first analyze the overall performance achieved for different subjects in Section A. And then, in Section B, we evaluate the influence of different frequency bands on the classification accuracy.
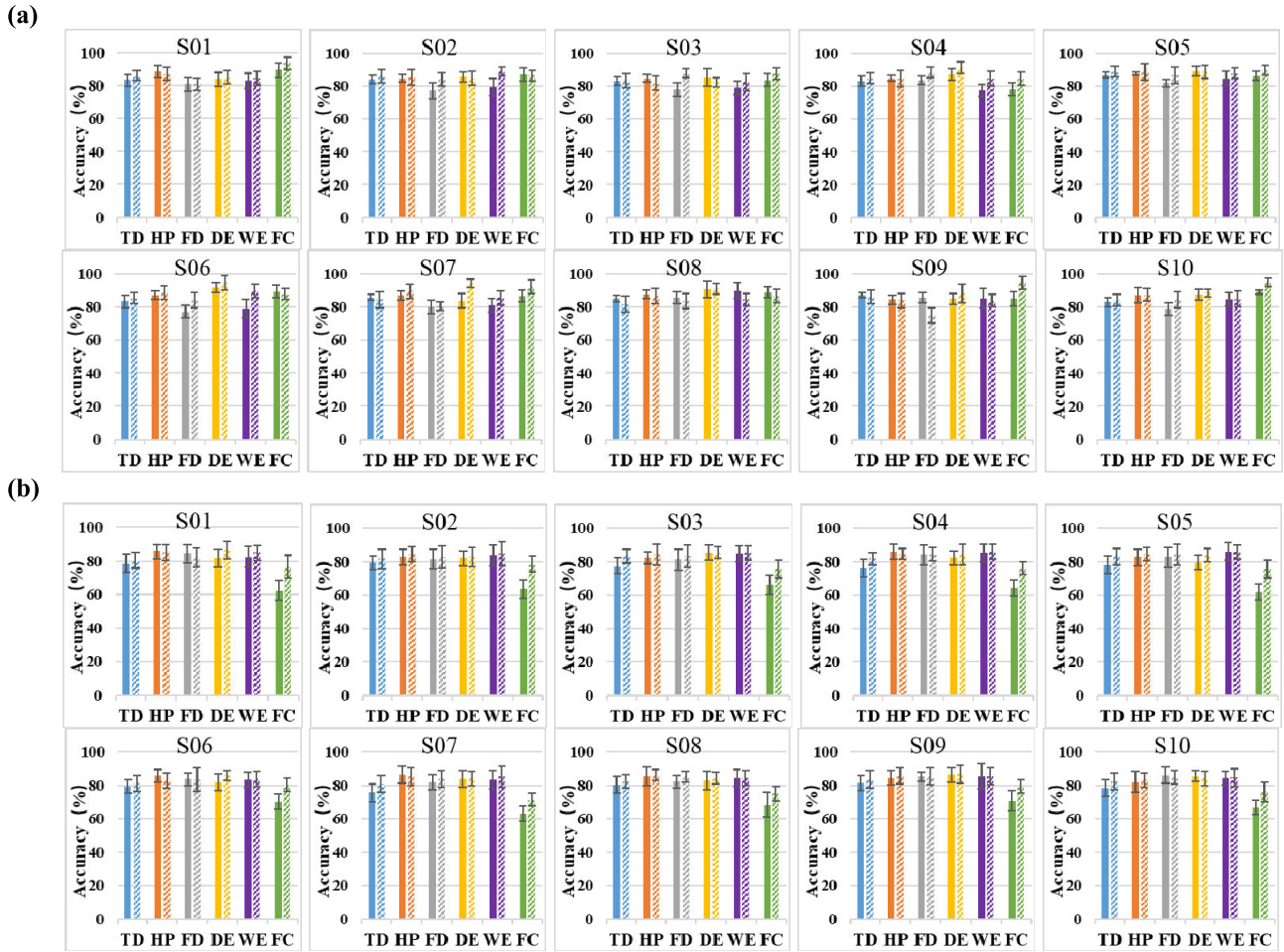
(a)

(b)

FIGURE 5. Classification results of first ten subjects using different features in DEAP (a) and TYUT2.0 (b).

A. OVERALL CLASSIFICATION RESULTS

First, we analyze the classification performance using different features of each subject in the DEAP and TYUT2.0 datasets. The classification results are shown in Fig. 5 and Fig. 6. The height of the bars marks the average accuracy whereas the whiskers mark the standard deviation. The plain colored bars and the hatched colored bars mark the performance of sensor space features and source space features, respectively.

In Fig. 5, while the classification performance varies with different subjects, for most subjects, the overall classification results tend to be similar across the mentioned features. Compared with the results obtained from sensor space features, it can be observed that the recognition results from source space features lead to a higher accuracy rate. Even though this improvement is not always systematic for all features, most of the features can achieve increased classification accuracy.

In this work, we can obtain the best accuracy rate of 94.82% with FC features of source space in the subject 10 from the DEAP dataset and 86.78% with DE features of source space in the subject 9 from TYUT 2.0 dataset separately. This result shows that features extracted from the

reconstructed cortex sources are superior to the ones from scalp EEG for emotion recognition. Moreover, the improved result is generally achieved from FC features, which reflects the fact that FC is more sensitive to the spatial resolution of brain signals.

In Fig. 6 (a), we can notice that the best result in the DEAP dataset is generally achieved for FC features, followed by DE, WE, HP, TD, and FD features. In Fig. 6 (b), the best result in the TYUT2.0 dataset is achieved for WE feature, followed by DE, HP, FD, TD, and FC features. In TYUT2.0, the features that exhibit the lowest accuracy is the FC with phase lag index, while it is difficult to detect the phase synchrony related to emotions based on the onset of each trial. In DEAP, the FC is extracted from the segments divided by the hamming window, which can keep the signal steady and avoid spectrum leakage.

B. INFUENCE OF DIFFERENT FREQUENCY BANDS

In section II, we have compared the significant differences between pairs of emotions for different frequency bands. While most of significant differences between pairs of emotions occur in γ-band, other significant differences

TABLE 3. Average classification accuracy and standard deviation of all subjects for individual frequency band in the DEAP and TYUT2.0.

Features		Sensor space				Source space			
		θ	α	β	γ	θ	α	β	γ
DEAP	DE	85.41 (3.76)	83.12 (3.96)	82.39 (3.94)	**85.92** (3.63)	87.17 (4.74)	85.39 (3.85)	86.47 (3.59)	**88.39** (3.14)
	FC	86.02 (2.68)	83.56 (3.20)	85.74 (3.14)	**88.49** (2.93)	88.79 (3.35)	88.60 (2.82)	86.65 (2.92)	**89.64** (3.10)
TYUT2.0	DE	83.51 (5.04)	82.34 (5.12)	82.55 (4.12)	**84.34** (4.91)	83.31 (4.05)	82.21 (4.69)	82.89 (44.87)	**84.67** (3.85)
	FC	66.91 (3.82)	**67.16** (3.75)	64.38 (4.24)	62.31 (3.37)	**73.08** (4.01)	72.55 (4.55)	71.63 (3.16)	72.71 (3.88)
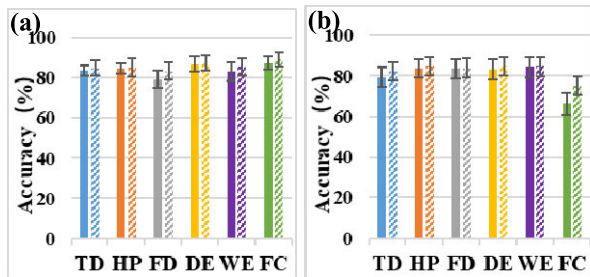
FIGURE 6. Average accuracy and standard deviation of all subjects using different features in DEAP (a) and TYUT2.0 (b).

are present in θ and α bands. Herein, we will analyze the classification accuracy in the DE and FC features with the individual frequency band. Table 3 shows the average classification accuracy and standard deviation of all subjects for an individual frequency band in DEAP and TYUT2.0. From the table, it can be observed that the best classification accuracy is achieved for DE and FC features in γ-band both sensor space and source space, except for the FC feature in TYUT2.0. And we can obtain the best average accuracy rate of 89.64% with FC features of source space in γ-band from the DEAP dataset and 84.67% with DE features of source space in γ-band from the TYUT 2.0 dataset separately. In the θ-band, the average accuracy yields a slightly lower value than γ-band. Overall, the classification results are consistent with the findings in section II, which show the significant active differences in γ and θ frequency bands.

IV. CONCLUSION

In this paper, we have analyzed the significant differences of active source regions and frequency bands for pairs of emotions-based reconstructed EEG sources using sLORETA, and 26 Brodmann areas are selected as the regions of interest (ROI). The selected ROI sets include BA3, 5, 6, 9, 10, 13, 18, 19, 23, 29, 30, 39 and 40 with bilateral hemispheres, which involve postcentral gyrus, prefrontal cortex, parietal cortex, temporal cortex and occipital cortex. Most significant differences between pairs of emotions occur in γ, θ and α bands. And then, six kinds of time- and frequency-domain features based on the current density of ROI are extracted to classify different emotions using support vector machines. Furthermore, we compare the classification performances of emotion features extracted from active source regions and EEG sensors on the DEAP and TYUT

2.0 EEG-based datasets. We have demonstrated that the features from selected source regions can improve the classification accuracy by extensive experiments. Moreover, the best classification accuracy is achieved for DE and FC features in γ-band both sensor space and source space. Because the reconstructed sources with sLORETA are blurred, as the future work, we need to explore a more accurate source localization method to improve emotion recognition performance further.

REFERENCES

[1] C. Mühl, B. Allison, A. Nijholt, and G. Chanel, "A survey of affective brain computer interfaces: Principles, state-of-the-art, and challenges," *Brain-Comput. Interfaces*, vol. 1, no. 2, pp. 66–84, Apr. 2014.

[2] S. M. Alarcao and M. J. Fonseca, "Emotions recognition using EEG signals: A survey," *IEEE Trans. Affect. Comput.*, vol. 10, no. 3, pp. 374–393, Jul. 2019.

[3] P. Ekman, "Basic emotions," in *Handbook of Cognition and Emotion*. Hoboken, NJ, USA: Wiley, 1999, pp. 45–60.

[4] H. Gunes and M. Pantic, "Automatic, dimensional and continuous emotion recognition," *Int. J. Synth. Emotions*, vol. 1, no. 1, pp. 68–99, Jan. 2010.

[5] T. Thanapattheerakul, K. Mao, and J. Amoranto, "Emotion in a century: A review of emotion recognition," in *Proc. 10th Int. Conf. Adv. Inf. Technol.*, 2018, p. 17.

[6] M. Egger, M. Ley, and S. Hanke, "Emotion recognition from physiological signal analysis: A review," *Electron. Notes Theor. Comput. Sci.*, vol. 343, pp. 35–55, May 2019.

[7] W. Zheng, "Multichannel EEG-based emotion recognition via group sparse canonical correlation analysis," *IEEE Trans. Cogn. Develop. Syst.*, vol. 9, no. 3, pp. 281–290, Sep. 2017.

[8] R. Majid Mehmood, R. Du, and H. J. Lee, "Optimal feature selection and deep learning ensembles method for emotion recognition from human brain EEG sensors," *IEEE Access*, vol. 5, pp. 14797–14806, 2017.

[9] M. Hassan and F. Wendling, "Electroencephalography source connectivity: Aiming for high resolution of brain networks in time and space," *IEEE Signal Process. Mag.*, vol. 35, no. 3, pp. 81–96, May 2018.

[10] H. Becker, L. Albera, P. Comon, R. Gribonval, F. Wendling, and I. Merlet, "Brain-source imaging: From sparse to tensor models," *IEEE Signal Process. Mag.*, vol. 32, no. 6, pp. 100–112, Nov. 2015.

[11] G. Lantz, R. G. De Peralta, L. Spinelli, and C. M. Michel, "Epileptic source localization with high density EEG: How many electrodes are needed?" *Clin. Neurophysiol.*, vol. 114, no. 1, pp. 63–69, 2003.

[12] C. M. Michel, M. M. Murray, G. Lantz, S. Gonzalez, L. Spinelli, and R. G. de Peralta, "EEG source imaging," *Clin. Neurophysiol.*, vol. 115, no. 10, pp. 2195–2222, Oct. 2004.

[13] A. Keil, M. M. Bradley, O. Hauk, B. Rockstroh, T. Elbert, and P. J. Lang, "Large-scale neural correlates of affective picture processing," *Psychophysiology*, vol. 39, no. 5, pp. 641–649, Sep. 2002.

[14] K. Keuper, P. Zwanzger, M. Nordt, A. Eden, I. Laeger, P. Zwitserlood, J. Kissler, M. Junghöfer, and C. Dobel, "How 'love' and 'hate' differ from 'sleep': Using combined electro/magnetoencephalographic data to reveal the sources of early cortical responses to emotional words," *Hum. Brain Mapping*, vol. 35, no. 3, pp. 875–888, 2014.

[15] G. Kashyap, M. Bora, M. Nishat, X. Cui, S.-H. Pun, and S. Barma, "Analysis of neural electrical activities during elicitation of human emotion based on EEG," in *Proc. Int. Conf. Signal Process. Commun. (ICSC)*, Dec. 2016, pp. 270–273.

[16] H. Becker, J. Fleureau, P. Guillotel, F. Wendling, I. Merlet, and L. Albera, "Emotion recognition based on high-resolution EEG recordings and reconstructed brain sources," *IEEE Trans. Affect. Comput.*, to be published.

[17] J. I. Padilla-Buritica, J. D. Martinez-Vargas, and G. Castellanos-Dominguez, "Emotion discrimination using spatially compact regions of interest extracted from imaging EEG activity," *Frontiers Comput. Neurosci.*, vol. 10, p. 55, Jul. 2016.

[18] A. Goshvarpour and A. Goshvarpour, "EEG spectral powers and source localization in depressing, sad, and fun music videos focusing on gender differences," *Cogn. Neurodyn.*, vol. 13, no. 2, pp. 161–173, Apr. 2019.

[19] J.-M. Schoffelen and J. Gross, "Source connectivity analysis with MEG and EEG," *Hum. Brain Mapping*, vol. 30, no. 6, pp. 1857–1865, Jun. 2009.

[20] S. Koelstra, C. Muhl, M. Soleymani, J. S. Lee, A. Yazdani, T. Ebrahimi, T. Pun, A. Nijholt, and I. Patras, "DEAP: A database for emotion analysis; Using physiological signals," *IEEE Trans. Affect. Comput.*, vol. 3, no. 1, pp. 18–31, Jan./Mar. 2011.

[21] J. Chang, X. Zhang, Q. Zhang, and Y. Sun, "Investigating duration effects of emotional speech stimuli in a tonal language by using event-related potentials," *IEEE Access*, vol. 6, pp. 13541–13554, 2018.

[22] R. D. Pascual-Marqui, "Standardized low-resolution brain electromagnetic tomography (sLORETA): Technical details," *Methods Find Exp. Clin. Pharmacol.*, vol. 24, pp. 5–12, Jan. 2002.

[23] M. Fuchs, J. Kastner, M. Wagner, S. Hawes, and J. S. Ebersole, "A standardized boundary element method volume conductor model," *Clin. Neurophysiol.*, vol. 113, pp. 702–712, May 2002.

[24] V. Jurcak, D. Tsuzuki, and I. Dan, "10/20, 10/10, and 10/5 systems revisited: Their validity as relative head-surface-based positioning systems," *NeuroImage*, vol. 34, no. 4, pp. 1600–1611, Feb. 2007.

[25] M. Bennett and P. Hacker, "Emotion and cortical-subcortical function: Conceptual developments," *Progr. Neurobiol.*, vol. 75, no. 1, pp. 29–52, Jan. 2005.

[26] L. Cao, J. Xu, X. Yang, X. Li, and B. Liu, "Abstract representations of emotions perceived from the face, body, and whole-person expressions in the left postcentral gyrus," *Frontiers Hum. Neurosci.*, vol. 12, pp. 419–432, Oct. 2018.

[27] M. J. Hofmann, L. Kuchinke, S. Tamm, M. L. H. Võ, and A. M. Jacobs, "Affective processing within 1/10th of a second: High arousal is necessary for early facilitative processing of negative but not positive words," *Cogn., Affect., Behav. Neurosci.*, vol. 9, no. 4, pp. 389–397, Dec. 2009.

[28] R. Jenke, A. Peer, and M. Buss, "Feature extraction and selection for emotion recognition from EEG," *IEEE Trans. Affect. Comput.*, vol. 5, no. 3, pp. 327–339, Jul. 2014.

[29] O. Sourina and Y. Liu, "A fractal-based algorithm of emotion recognition from EEG using arousal-valence model," in *Proc. Int. Conf. Bio-Inspired Syst. Signal Process. (BIOSIGNALS)*, Jan. 2011, pp. 209–214.

[30] L.-C. Shi, Y.-Y. Jiao, and B.-L. Lu, "Differential entropy feature for EEG-based vigilance estimation," in *Proc. 35th Annu. Int. Conf. IEEE Eng. Med. Biol. Soc. (EMBC)*, Jul. 2013, pp. 6627–6630.

[31] O. A. Rosso, S. Blanco, J. Yordanova, V. Kolev, A. Figliola, M. Schürmann, and E. Başar, "Wavelet entropy: A new tool for analysis of short duration brain electrical signals," *J. Neurosci. Methods*, vol. 105, no. 1, pp. 65–75, Jan. 2001.

[32] R. Quian Quiroga, O. A. Rosso, E. Başar, and M. Schürmann, "Wavelet entropy in event-related potentials: A new method shows ordering of EEG oscillations," *Biological*, vol. 84, no. 4, pp. 291–299, Mar. 2001.

[33] Y.-Y. Lee and S. Hsieh, "Classifying different emotional states by means of eeg-based functional connectivity patterns," *PLoS ONE*, vol. 9, no. 4, Apr. 2014, Art. no. e95415.

[34] M. Hassan, O. Dufor, I. Merlet, C. Berrou, and F. Wendling, "EEG source connectivity analysis: From dense array recordings to brain networks," *PLoS ONE*, vol. 9, no. 8, Aug. 2014, Art. no. e105041.

[35] C. J. Stam, G. Nolte, and A. Daffertshofer, "Phase lag index: Assessment of functional connectivity from multi channel EEG and MEG with diminished bias from common sources," *Hum. Brain Mapping*, vol. 28, no. 11, pp. 1178–1193, Nov. 2007.

[36] S. Aydore, D. Pantazis, and R. M. Leahy, "A note on the phase locking value and its properties," *NeuroImage*, vol. 74, pp. 231–244, Jul. 2013.

[37] M. Rubinov and O. Sporns, "Complex network measures of brain connectivity: Uses and interpretations," *NeuroImage*, vol. 52, no. 3, pp. 1059–1069, Sep. 2010.

[38] S. S. Keerthi and C.-J. Lin, "Asymptotic behaviors of support vector machines with Gaussian Kernel," *Neural Comput.*, vol. 15, no. 7, pp. 1667–1689, Jul. 2003.

[39] G. Chen, X. Zhang, Z. J. Wang, and F. Li, "An enhanced artificial bee colony-based support vector machine for image-based fault detection," *Math. Problems Eng.*, vol. 2015, pp. 1–12, 2015.

[40] C.-C. Chang and C. J. Lin, "LIBSVM: A library for support vector machines," *ACM Trans. Intell. Syst. Technol.*, vol. 2, no. 3, p. 27, 2011.

GUIJUN CHEN received the B.S. and Ph.D. degrees from the Taiyuan University of Technology, China, in 2010 and 2016, respectively. He is currently a Lecturer with the College of Information and Computer, Taiyuan University of Technology. His research interests are in the areas of intelligent information processing, bio-medical imaging, electroencephalography (EEG) signal analysis, and brain–machine interfaces.

XUEYING ZHANG (Member, IEEE) received the Ph.D. degree in underwater acoustic engineering from Harbin Engineering University, in 1998. She is currently a Professor with the Taiyuan University of Technology. She has supervised a lot of national, province, or ministry research projects. She has published over 100 articles in the periodicals of national level and international conferences and about 40 articles were indexed by SCI, EI, or ISTP. Her research interests include auditory model, emotional speech recognition, and machine learning.

YING SUN received the Ph.D. degree in engineering from the Taiyuan University of Technology, Shanxi, China. She is currently an Associate Professor with the Taiyuan University of Technology. Her research interests are mainly in the areas of speech signal processing and speech emotion recognition. She has published more than ten articles in periodicals of national level and international conferences. About four articles were indexed by SCI, EI, or ISTP. Two of province research projects have been finished by her supervising.

JING ZHANG received the B.S. degree from the North University of China, in 2014, and the M.E. degree from the Taiyuan University of Science and Technology, Taiyuan, China, in 2018. He is currently pursuing the Ph.D. degree with the Institute of Digital Media and Communication, Taiyuan University of Science (TYUT), Taiyuan. His researches focus on affective computing, machine learning, pattern recognition, and image processing.

• • •